Influence of Supercurrents on Low-Temperature Thermopower in Mesoscopic N/S Structures

J. Zou[1], I. Sosnin[1], P. Virtanen[2], M. Meschke[2], V. T. Petrashov[1], and T. T. Heikkilä[2]

[1]*Physics Department, Royal Holloway University of London, Egham, Surrey, TW20 0EX, U.K.*
[2]*Low Temperature Laboratory, Helsinki University of Technology, P.O. Box 2200, FIN-02015 HUT, Finland*

The thermopower of mesoscopic normal metal/superconductor structures has been measured at low temperatures. Effect of supercurrent present in normal part of the structure was studied in two cases: when it was created by applied external magnetic field and when it was applied directly using extra superconducting electrodes. Temperature and magnetic field dependencies of thermopower are compared to the numerical simulations based on the quasi-classical theory of the superconducting proximity effect.

PACS numbers: 73.50. Lw, 74.25. Fy, 74.50.+r

1. Introduction

Thermoelectric properties of hybrid normal-metal/superconductor (N/S) structures are strongly modified by the superconducting proximity effect (see Refs. 1,2 for review). It was predicted that at low temperatures the thermopower in mesoscopic N/S structures can be as much as 1000 times larger than that in normal metals.[3] Moreover, the thermopower acquires a phase-coherent part as was first observed in Ref. 4, where thermopower oscillations as a function of superconducting phase difference ϕ were recorded in a geometry of an Andreev intereferometer (a superconducting loop connected to a normal part, see review[5] for details). According to theory,[6,7] this oscillating part of thermopower should be antisymmetric in ϕ and have reentrance in temperature dependence with a maximum at the Thouless energy, similar

to that of magnetoresistance.[1] The value of thermopower at the maximum can reach a few μV/K. It is worth mentioning that in quantitative measurements of thermopower,[8] where local thermometry technique based on proximity resistance[9] was used, the value of only 100nV/K was reported, considerably less than that predicted by theory. While the above qualitative behavior has been observed in several experiments, some deviations from it have been reported as well. In particular, large thermopower symmetric in ϕ has been observed,[4,10] which is not explained by theory. Close to the superconducting transition of the superconducting parts of hybrid mesoscopic NS junctions, a thermopower due to quasiparticle thermoelectric currents has been reported.[11,12] However, the value of the thermopower observed near T_c in these experiments was considerably larger than that predicted by theory.[13] In structures consisting of a normal ring with only one superconducting contact a small thermopower periodic and symmetric with respect to magnetic flux through the normal ring has been reported.[14] Recently, thermal conductivity of Andreev interferometers has been studied as well, see Refs. 15,16.

In this paper we concentrate on the effect of supercurrents flowing through the normal part of the Andreev interferometer, which were first highlighted in Ref. 7. We designed our structure so that the supercurrent can be created by an applied magnetic flux through the superconducting loop or directly from an external power supply using extra superconducting contacts. The results are compared with the predictions from the quasiclassical theory.

2. Sample fabrication and Measurement

The samples were fabricated using two-stage e-beam lithography. First, a normal part was made of a thermally evaporated 30 nm thick Ag film. Then the second layer was made of 55nm thick Al film used as a superconductor. To obtain clean interfaces between the layers, the contact area was Ar^+ plasma etched before the deposition of the second layer. This $in-situ$ etching process produces interface resistance less than 1 Ω for contact area of 100nm $\times$ 200nm. Figure 1 shows the geometry of one of the measured samples. The sample consists of an H-shaped N wire connected to a superconducting loop with two S contacts, S_1 and S_2, and to superconducting contacts S_3 and S_4. On the left side, the N structure is connected to a

---

[1]Although, in the previous case the Thouless energy $E_T = \hbar D/L^2$ is determined from the distance L between the superconductors, and in the latter case from the distance of the superconductors to the normal terminals.
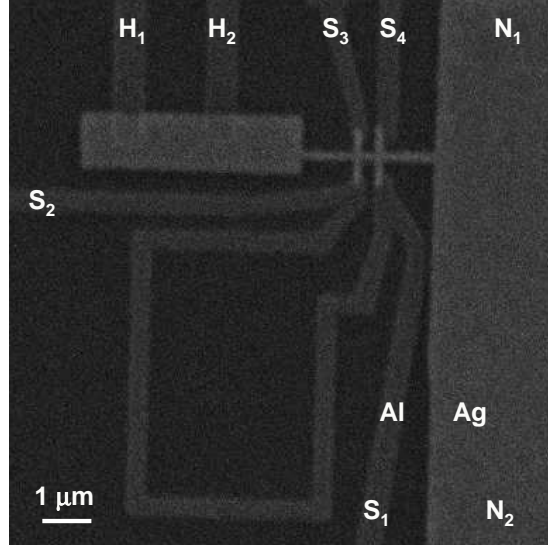
Fig. 1. SEM micrograph of the measured sample.

small normal reservoir (which we will call a quasi-reservoir), which in turn is connected to two superconductor electrodes H_1 and H_2. By passing current from H_1 to H_2 we were able to vary the temperature of the quasi-reservoir. On the right side the N structure is connected to a normal reservoir, which is in good thermal contact with massive Au pads so that its temperature is fixed by the substrate.

Measurements were performed in a He^3 cryostat at temperatures from 0.28 K to 1.5 K with a magnetic field up to 1 mT applied perpendicular to the substrate. Resistivity, ρ, of the Ag film was about 2 $\mu\Omega$cm with diffusion constants, D, about 130 cm^2/s.

Magnetoresistance measurements were performed using conventional ac bridge technique. Thermopower measurements have been done using two different methods. In the first method, a heating current, I_h, was a sum of dc and 0.5μA ac currents and it was applied between H_1 and H_2. Thermovoltage, V_{th}, between S_2 and N_1 was measured using a lock-in amplifier on the frequency of the ac signal. In the second method, only ac current at the frequency f was applied to the heater but the signal was measured by the lock-in amplifier at the frequency $2f$. A superconducting magnet was used to sweep a magnetic field. Zero of magnetic field on all graphs corresponds to zero current through the magnet. Since there was a small shift due to magnetic field of the Earth, the relative phase of thermopower and magnetoresistance oscillations was double checked by repeated measurements to

ensure they were measured with the same reference point.

3. Theory

Nonequilibrium electrical properties of diffusive superconductor – normal-metal heterostructures can be described with the quasiclassical Keldysh-Usadel theory.[2,20,21,23] We model the experimental sample by a system of quasi-one-dimensional wires connected to each other at nodes, see Fig. 2. The primary object to be described is the Keldysh Green's function,

$$\check{G}(E,x) = \begin{pmatrix} \hat{G}^R(E,x) & \hat{G}^K(E,x) \\ 0 & \hat{G}^A(E,x) \end{pmatrix}, \ \hat{G}^A = -\hat{\tau}_3(\hat{G}^R)^\dagger\hat{\tau}_3, \ \hat{G}^K = \hat{G}^R\hat{h} - \hat{h}\hat{G}^A,$$

(1)

where $\hat{G}^R$, $\hat{G}^A$, and $\hat{G}^K$ are the Retarded, Advanced and Keldysh Green functions, $\hat{h} \equiv f_L\hat{1} + f_T\hat{\tau}_3$ describes two degrees of freedom of the distribution function, and $\hat{\tau}_i$ is the i:the Pauli matrix. Each of these is a 2×2 matrix in the Nambu particle-hole space. In addition, $\hat{G}^R$ and $\hat{G}^A$ satisfy the normalization condition $(\hat{G}^R)^2 = (\hat{G}^A)^2 = \hat{I}$, where $\hat{I}$ is the identity matrix. In this notation, symbols with a "check" (such as $\check{G}$) are chosen to represent matrices in the Keldysh space, and symbols with a "hat" ($\hat{G}$) are matrices in the Nambu space.

Usadel equation for $\check{G}(E,x)$, combined with the boundary conditions in the reservoirs and the nodal conditions, is essentially a circuit theory for matrix currents

$$\check{I}_i \equiv \sigma_i A_i \check{G}\underline{\nabla}\check{G}$$

flowing in each wire i. Here $\sigma_i = e^2\nu_{F,i}D_i$ is the normal-state conductivity, A_i the cross section, $\nu_{F,i}$ the density of states and D_i the diffusion constant of wire i. The gauge-invariant gradient is denoted as $\underline{\nabla}\check{G} \equiv \nabla\check{G} - ie\mathbf{A}[\hat{\tau}_3, \check{G}]$, where $\mathbf{A}$ is the vector potential. Not all parts of this current are conserved, but there are leakage terms due to the finite energy and due to inelastic scattering,

$$\underline{\nabla} \cdot \check{I}_i = e^2\nu_F[-iE\check{\tau}_3 + \check{\Sigma}_{\text{in}}, \check{G}]. \tag{2}$$

Here $\check{\tau}_3 = \hat{\tau}_3 \otimes \check{I}$. This form is valid in a normal metal where the superconducting order parameter Δ vanishes. The first leakage term describes the dissociation of Cooper pairs entering a normal metal, and it gives the finite penetration depth $\xi_E = \sqrt{\hbar D/E}$ for the proximity effect. The second term $\check{\Sigma}_{\text{in}}$ describes inelastic scattering due to, for example, electron-electron or electron-phonon interaction. In what follows, we assume that the latter term is finite only in the electrodes and vanishes inside the wires.

Low-temperature thermopower in mesoscopic N/S structures

The matrix currents flowing at different wires are connected via the nodal conditions: the sum of the currents $\check{I}_i$ flowing into each node vanishes and the functions $\check{G}$ are continuous across each node.

For the numerics, it is convenient to parametrize the Retarded and Advanced Green's function by the complex parameters θ and χ, such that

$$\hat{G}^R = \cosh(\theta)\hat{\tau}_3 + \sinh(\theta)(\cos(\chi)i\hat{\tau}_2 + \sin(\chi)i\hat{\tau}_1) \tag{3a}$$

$$\hat{G}^A = -\cosh(\bar{\theta})\hat{\tau}_3 - \sinh(\bar{\theta})(\cos(\bar{\chi})i\hat{\tau}_2 + \sin(\bar{\chi})i\hat{\tau}_1). \tag{3b}$$

Here $\bar{\theta}$ and $\bar{\chi}$ are the complex conjugates of θ and χ. With this parametrization, Eq. (2) can be broken into four scalar equations, two for the Retarded/Advanced parts,

$$D\nabla^2\theta = -2i(E + i0^+)\sinh(\theta) + \frac{1}{2D}v_S^2\sinh(2\theta), \tag{4a}$$

$$D\nabla \cdot j_E = 0, \quad Dj_E \equiv -\sinh^2(\theta)v_S, \quad v_S \equiv D(\nabla\chi - 2eA/\hbar). \tag{4b}$$

and two for the Keldysh part,

$$D\nabla \cdot j_L = 0, \qquad j_L \equiv -\mathcal{D}_L\nabla f_L - \mathcal{T}\nabla f_T + j_S f_T, \tag{5a}$$

$$D\nabla \cdot j_T = 0, \qquad j_T \equiv -\mathcal{D}_T\nabla f_T + \mathcal{T}\nabla f_L + j_S f_L. \tag{5b}$$

Equations (4) describe the spectral properties of the system and from their solution, one finds the local density of states, energy and position dependent diffusion constants, and the spectral supercurrent. The latter two, Eqs. (5) are the kinetic equations, which describe the behavior of the distribution functions f_L and f_T. They can be expressed in forms of static continuity equations for the spectral (energy dependent) energy and charge currents j_L and j_T. The coefficients of these equations are obtained from the solutions of the spectral equations,

$$\mathcal{D}_L \equiv \frac{1}{4}\text{Tr}[1 - \hat{G}^R\hat{G}^A] = \frac{1}{2}(1 + |\cosh\theta|^2 - |\sinh\theta|^2\cosh(2\text{Im}[\chi])), \tag{6a}$$

$$\mathcal{D}_T \equiv \frac{1}{4}\text{Tr}[1 - \hat{G}^R\hat{\tau}_3\hat{G}^A\hat{\tau}_3] = \frac{1}{2}(1 + |\cosh\theta|^2 + |\sinh\theta|^2\cosh(2\text{Im}[\chi])), \tag{6b}$$

$$\mathcal{T} \equiv \frac{1}{4}\text{Tr}[\hat{G}^A\hat{G}^R\hat{\tau}_3] = \frac{1}{2}|\sinh\theta|^2\sinh(2\text{Im}[\chi])), \tag{6c}$$

$$j_S \equiv \frac{1}{4}\text{Tr}[(\hat{G}^R\underline{\nabla}\hat{G}^R - \hat{G}^A\underline{\nabla}\hat{G}^A)\hat{\tau}_3] = \text{Im}[-\sinh^2(\theta)v_S]/D = \text{Im}[j_E]. \tag{6d}$$

Here $\mathcal{D}_L$ and $\mathcal{D}_T$ are the spectral energy and charge diffusion constants, $\mathcal{T}$ is an anomalous kinetic coefficient which is finite only in the presence of the supercurrent, and j_S is the spectral supercurrent.

Finally, in the reservoirs the Green functions tend into the bulk functions of those reservoirs. For Retarded/Advanced parts in the absence of magnetic field this means $\hat{G}^R = -\hat{G}^A = \hat{\tau}_3$ or $\theta = 0$ in a normal metal and they tend to $\hat{G}^R = g\hat{\tau}_3 + f(\cos(\phi)i\hat{\tau}_2 + \sin(\phi)i\hat{\tau}_1)$in a superconductor with the superconducting order parameter $\Delta = |\Delta|e^{i\phi}$, with

$$g = \frac{|E|}{\sqrt{(E + i0^+)^2 - |\Delta|^2}}, \quad f = \frac{\Delta \, \mathrm{sgn} E}{\sqrt{(E + i0^+)^2 - |\Delta|^2}} ,$$

or $\theta = \mathrm{artanh}(|\Delta|/\mathrm{E})$ and $\chi = \phi$.

The reservoir values for the distribution functions $f_{L/T}$ are given by

$$f_{L/T}^0 = \frac{1}{2}\left(\tanh\left(\frac{E + eV}{2k_B T}\right) \pm \tanh\left(\frac{E - eV}{2k_B T}\right)\right),$$

where eV is the potential and T is the temperature of the reservoir. There is one exception: for energies below the superconducting gap, Andreev reflection forbids the energy current into a superconductor. Therefore, there the Dirichlet boundary condition of $f_L = f_L^0$ is changed into the vanishing of the energy current, $j_L = 0$ into all superconductors.

If one would like to describe the behavior of the superconducting order parameter Δ in the superconducting parts of the structure, a self-consistency equation connecting Δ with the solution $\{\theta, \chi, f_L, f_T\}$ could be applied. However, in what follows we assume that all the superconductors are reservoirs, such that Δ obtains its bulk value quickly near the NS boundary. Such an assumption works fairly well for our system, but it brings some inaccuracy to the exact position of the NS interface as the inverse proximity effect suppresses Δ and θ close to the interface. Generally these quantities have a healing length of the order of the superconducting coherence length, $\xi_0 = \sqrt{\hbar D/(2\Delta)}$.

Another consequence of assuming that the superconductors are reservoirs is a boundary condition $f_T = 0$ at the normal-superconducting interface. For energies below the gap, f_T decays into the superconductors within ξ_0, but above the gap, the decay length is much longer, of the order of the charge relaxation length inside the superconductors.[24] The validity of this assumption may thus be questionable at high temperatures, where thermal quasiparticles inside superconductors play a role. To simulate the effect of a very long charge relaxation length, we replaced the Dirichlet boundary condition for the distribution functions at $E > \Delta$ with a Neumann condition $\partial_x f_L = \partial_x f_T = 0$. This then takes into account the charge-imbalance voltage due to the quasiparticle current entering the superconductor, assuming the detailed form of charge relaxation can be neglected. Compared to the

Low-temperature thermopower in mesoscopic N/S structures

$$V = 0, \; T_0, \; -\phi_S/2 \qquad V = 0, \; T_0, \; \phi_S/2$$

$$V = 0, \; T_0, \qquad V = 0, \; T_0,$$
$$(\phi_z - \phi_{\text{loop}})/2 \qquad (\phi_z + \phi_{\text{loop}})/2$$
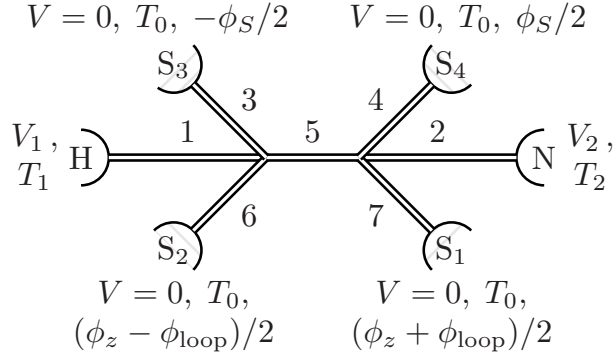
Fig. 2. Schematic system considered in the numerics. Major features of the experiments can be attributed to the effect of phase gradients across the superconducting interfaces on the various observables of the system. The phase ϕ_z is fixed by current conservation, $I_6 = -I_7$; for a left-right symmetric system $\phi_z = 0$. The phase ϕ_{loop} can be controlled by the flux through the superconducting loop, and ϕ_S by the applied supercurrent between the contacts S_3 and S_4.

Dirichlet condition, this condition results in our geometry to a slightly reduced thermopower at high temperatures, where thermal quasiparticles play a role.

Equations (4) and (5) together with the nodal and boundary conditions need in general to be solved numerically. When the solutions to them are found, one can obtain, for example, the observable energy and charge currents flowing in wire i from

$$I_{Q,i} = \frac{A_i \sigma_i}{e^2} \int_0^\infty dE j_{L,i} \tag{7}$$

$$I_{C,i} = \frac{A_i \sigma_i}{e} \int_0^\infty dE j_{T,i}. \tag{8}$$

The current conservation and Kirchoff laws for these currents follow naturally from the corresponding laws for $j_{L/T}$.

The numerical results presented in the remainder of this text have been obtained by solving the above equations without further approximations. We model the experimental setup with the schematic system presented in Fig. 2, where seven quasi-one-dimensional wires are connected to each other and to two normal-metal and four superconducting reservoirs. The lengths and areas of the different wires are estimated from the SEM picture and the resistances of each wire, as most of the latter can be separately measured. Thus, we estimate $L_1 = 1.44\mu$m, $L_2 = 1\mu$m, $L_3 \approx L_4 = 340$nm, and $L_5 = 460$nm, $w_1 = 120$nm, $w_2 = 160$nm, $w_3 \approx w_4 = 100$nm, and

$w_5 = 100$nm, where L_i are the lengths and w_i are the widths of the different wires. Thickness of the wires was assumed constant. This corresponds to the resistances $R_1 = 7.9\Omega$, $R_2 = 4.1\Omega$, $R_3 \approx R_4 = 2.2\Omega$, and $R_5 = 3\Omega$. In R_1, we included also the resistance 0.8Ω of the quasireservoir. As the parameters for the wires 6 and 7 could not be separately measured, we assume the system symmetric with respect to the inversion around the around the axis lying along wires 1, 5, and 2. In all the numerical curves, we use the same set of parameters, and fit only the diffusion constant D and the self-inductance L of the superconducting loop, see below.

We aim to calculate two separately measured observables for the same measured structure: the critical supercurrent $I_C(T)$ between the superconductors S_3 and S_4 and the thermopower $Q \equiv (V_2 - V_S)/(T_2 - T_1)|_{I_1=I_2=0}$ between reservoir 2 and the superconductors.

As shown for example in Refs. 7,2, the presence of the spectral supercurrent and the anomalous kinetic coefficient in Eqs. (5) may lead to a finite thermopower. In the limit where the energy scales of the system are far below Δ, there is also an approximate relation between the induced potentials and the supercurrent flowing in the system,

$$\mu_{\mathrm{sc},1/2} = \frac{e}{2} \frac{R_5(2R_{4/3} + R_5)R_{3/4}(I_S(T_1) - I_S(T_2))}{(R_1 + R_2 + R_5)(R_3 + R_4 + R_5)}$$
$$= 0.58 \ \Omega \ e \ (I_S(T_1) - I_S(T_2)). \tag{9}$$

The numerical value in Eq. (13) is specific to the geometry of the present system.

It turns out that the phase difference ϕ between the two NS interfaces S_1 and S_2 and the total flux through the superconducting loop are not linearly proportional to each other, but one has to take into account both the kinetic and geometric inductance of the loop to find their relation, as was shown in Ref. 25. The former is found using the consistency equation (see for example Ref. 27)

$$I_6(\phi) = I_{\mathrm{loop}}(\phi). \tag{10}$$

To find $\phi(\Phi)$, we can as a first step assume that the phase gradient in the loop is small and approximate

$$I_{\mathrm{loop}}(\phi) \approx \frac{\pi|\Delta|}{2} \tanh \frac{|\Delta|}{2k_B T} \frac{A\sigma v_S}{D}, \quad \frac{A\sigma v_S}{D} \approx \frac{2\pi n - \phi + 2\pi\Phi/\Phi_0}{eR_{N,loop}}, \tag{11}$$

where $2\pi n - \phi + \Phi/\Phi_0$ $(n \in \mathbb{Z})$ is the gauge-invariant phase difference over the superconducting part of the loop, Φ the total flux through it and $\Phi_0 = h/(2e)$ is the flux quantum. The prefactor in front of v_S is found by solving

the Usadel equation inside a bulk superconductor. Applying Eq. (10) now implies that

$$\phi = 2\pi \frac{\Phi}{\Phi_0} + 2\pi n - \frac{2e}{\hbar} L_K I_3(\phi), \quad L_K \equiv \frac{\hbar R_{N,loop}}{\pi |\Delta|} \left[\tanh \frac{|\Delta|}{2k_B T} \right]^{-1}. \quad (12)$$

In our structure, assuming $R_{N,loop} \sim 20\,\Omega$, and $|\Delta|/k_B \sim 2\,\mathrm{K}$ yields a kinetic inductance $L_K \sim 20\,\mathrm{pH}$ at $k_B T \ll |\Delta|$. However, one should also take into account the geometric self-inductance L_{geom} of the SQUID, which modifies the relation between Φ and the external flux. Hence, the true phase difference between the superconductors is found from

$$2\pi \frac{\Phi_x}{\Phi_0} \,(\mathrm{mod}\,2\pi) - \phi = \frac{2e}{\hbar}(L_K + L_{\mathrm{geom}})I(\phi) = \frac{2e}{\hbar} LI(\phi). \quad (13)$$

In what follows, for each external flux Φ_x, we calculate the phase ϕ by solving Eq. (13) numerically. It turns out (see below) that the results are well fitted with the loop inductance $L \approx 50$ pH. For a circular loop of radius $R \approx 2.4\,\mu\mathrm{m}$ and cross section $A_l = 35\mathrm{nm} \times 400\,\mathrm{nm}$, we would estimate a geometric self-inductance $L_{\mathrm{geom}} = \mu_0 R[\ln(8R/A_l) - 7/4] = 21$ pH, so that the sum $L_K + L_{\mathrm{geom}} = 40\,\mathrm{pH}$ is comparable to the fitted value.

It is straightforward to verify that the Usadel equations (4–5) remain invariant under the transformation

$$\chi \mapsto -\chi, \quad \mathbf{A} \mapsto -\mathbf{A}, \quad f_T \mapsto -f_T, \quad j_T \mapsto -j_T, \quad (14)$$

also inside the superconductors. Moreover, it turns out that this symmetry is shared by Eq. (13) and the self-consistency condition, provided that $\Delta = |\Delta|e^{i\phi} \mapsto |\Delta|e^{-i\phi}$. This implies that for any given solution of the problem, there is a second solution with inverted magnetic and electric fields, corresponding to charge and supercurrents flowing in the opposite direction. For the thermopower this implies that between any pair of reservoirs,

$$Q \equiv \left. \frac{\Delta V(\phi)}{\Delta T(\phi)} \right|_{I_C=0} = \left. \frac{-\Delta V(-\phi)}{\Delta T(-\phi)} \right|_{-I_C=0} = -\left. \frac{\Delta V(-\phi)}{\Delta T(-\phi)} \right|_{I_C=0}, \quad (15)$$

i.e., that its phase oscillations are always antisymmetric. This is a general symmetry of the quasiclassical model in a static situation, valid in a finite magnetic field and also when superconductors are treated self-consistently.

This symmetry is in contrast with the $\cos(\phi)$-dependent thermopower measured in Refs. 4,10, or the constant offset thermopower measured in Ref. 14. At present we do not know a reason for this discrepancy.
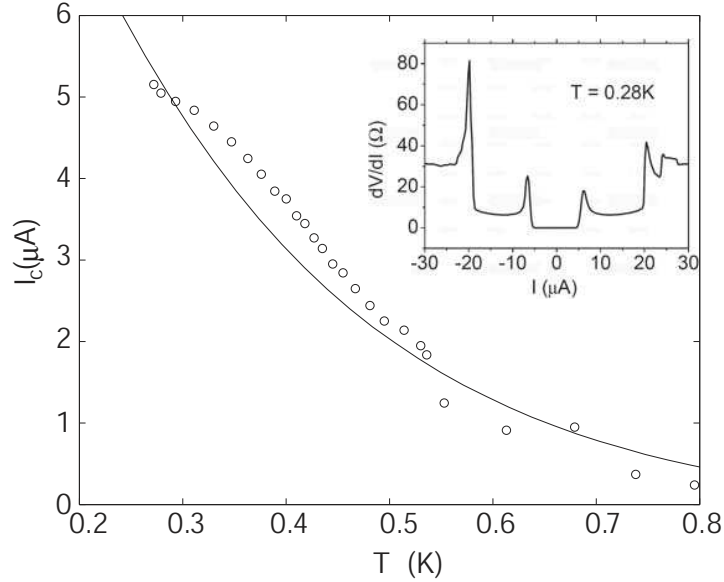
Fig. 3. Critical current I_c of the SNS junction as a function of temperature. Dots: measured I_c, solid line: fit to the theory (see text). Inset: Differential $I-V$ curve of the SNS junction at $T = 0.28$ K measured using S_3-S_4.

4. Experimental data

Below we present experimental data for thermopower and resistance measurements in the presence of temperature gradients created by heater currents. To avoid heat leak into electrodes H_1 and H_2 we kept $I_h < I_c$, where I_c is the critical current of the superconducting transition for heater electrodes H_1 and H_2. We measured current-voltage characteristic (I-V) of H_1-H_2 and found $I_c = 25\mu A$, so I_h smaller than $10\mu A$ was used to ensure contacts H_1 and H_2 are in the superconducting state.

To characterize the SNS junction, we measured its critical current at different temperatures. Inset of Fig. 3 shows differential $I-V$ curve of the SNS junction measured using contacts S_3-S_4 at T=0.28K. The jump at high currents corresponds to the superconducting transition of the parts of Al contacts S_3-S_4, while the second jump at smaller currents corresponds to the superconducting transition of normal parts L_3, L_5, and L_4. The critical current was measured as the current value at $dV/dI=R_N/2$, where $R_N \approx 6.3\Omega$ is the value of resistance of L_3-L_5-L_4 in normal state. Asymmetry in dV/dI curve can be attributed to the difference in Joule heat released in the wires when the superconducting transition is approached from normal state (negative currents in Fig. 3, inset) and that when it is approached from the superconducting state (positive currents in Fig. 3, inset). The

temperature dependence of I_c is plotted in Fig. 3. A numerical best fit, based on the quasiclassical theory presented above, to this data is given as a solid line, which also includes the temperature dependence of the gap $\Delta(T)$. We used low temperature value of the gap $\Delta(0)/k_B \approx 2K$ estimated from the superconducting transition temperature of Al wires. In this fit, we found the Thouless energy $E_T \approx 50\text{mK}/k_B$ that best corresponds to the measured temperature dependence. The fitted Thouless energy corresponds to a diffusion constant $D \approx 85\text{cm}^2/\text{s}$, in accordance to the value estimated from resistivity.
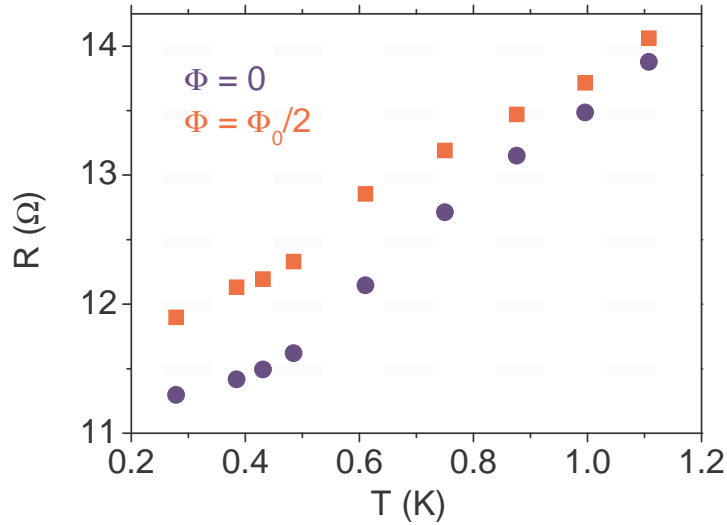
Fig. 4. (Color online): Amplitude of magnetoresistance oscillations measured with current probes H_1-N_1 and potential probes H_2-N_2. Circles correspond to resistance minimum, squares, to maximum.

Figure 4 shows temperature dependence of the resistance measured using current contacts H_1-N_1 and potential contacts H_2-N_2 (see Fig. 1) at different values of magnetic flux through the S loop. The bottom curve is for $\Phi = 0$ and the top one is for $\Phi = \Phi_0/2$. At a fixed temperature the resistance oscillates between these two values as a function of the applied magnetic flux, see Fig. 5b. The amplitude of the oscillations is affected by the screening effect discussed in Ref. 25,26. The screening effect was also seen directly as deviation of the shape of magnetoresistance oscillations from sinusoidal form, see Fig. 5. Figure 5 shows magnetoresistance and thermopower oscillations at the same temperature. The magnetoresistance was measured

using current probes H_1-N_1 and voltage probes H_2-N_2. Thermovoltage was measured using heater current applied to heaters H_1-H_2. For thermopower measurements presented here the heater current was a sum of 4 μA dc and 0.5 μA ac components. The signal was then measured by the lock-in amplifier at the frequency of ac modulation between contacts S_2-N_1. Note that thermovoltage oscillations are antisymmetric with respect to the direction of magnetic field, in contrast to magnetoresistance oscillations (this is seen directly from phase shift of $\pi/2$ for thermovoltage oscillations compared to that of magnetoresistance).
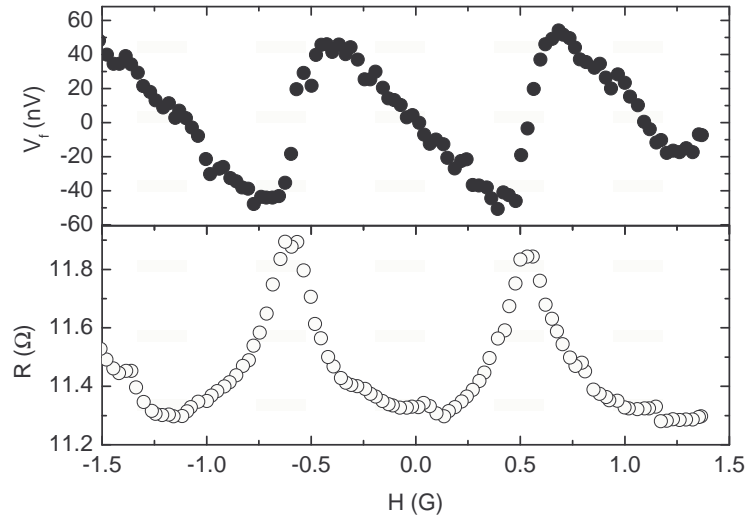
Fig. 5. Top: Thermovoltage oscillations measured at $T = 0.28$ K with heater current H_1-H_2 and voltage probes S_2-N_1. Bottom: magnetoresistance oscillations measured at $T = 0.28$ K using current probes H_1-N_1 and voltage probes H_2-N_2.

Non-sinusoidal shape of magnetoresistance oscillations indicates the presence of supercurrent in the normal part of the hybrid superconducting loop. Indeed, direct measurement of I-V curves of the central N-wire using contacts S_3-S_4 confirms this (see Fig. 3) and gives us an estimate of the magnitude of this supercurrent at different temperatures: the SNS structures formed by the superconducting loop and its contacts to the normal-metal wires are very similar to that formed by the S_3-S_4 contacts. We may thus estimate the effect of screening from the shape of the thermovoltage oscillations, using the fitted value of the supercurrent. Figure 6 shows the mea-

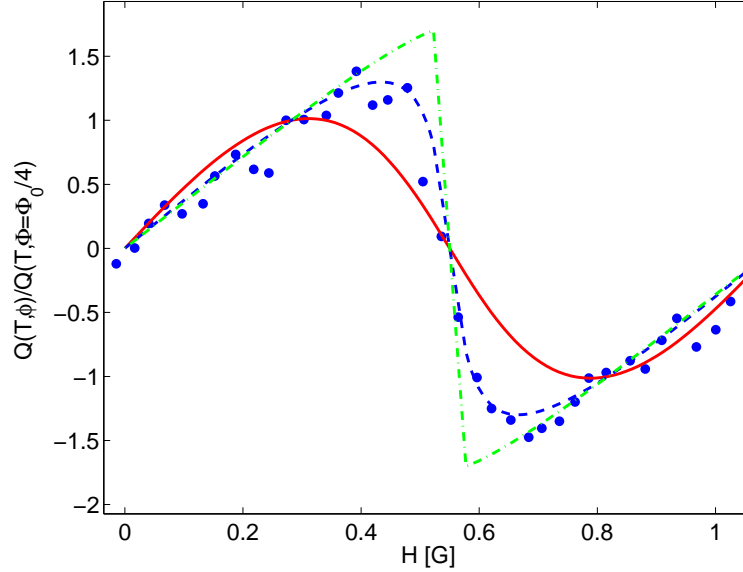**Low-temperature thermopower in mesoscopic N/S structures**

Fig. 6. (Color online): Thermovoltage oscillations (filled circles) measured at $T = 0.28$ K with heater current H_1-H_2 and voltage probes S_2-N_1. Theoretical fits to the shape of the oscillations with different values of the loop self-inductance: $L = 0$ (solid line), $L = 50$ pH (dashed line) and $L = 100$ pH (dash-dotted line).

sured thermovoltage oscillations along with three theory curves calculated with different loop inductances. Note that the amplitude of the theory curves are scaled to the experimental data, so one should only pay attention to the shape of the oscillations. The temperature dependence of the measured thermopower amplitude is compared to the theory in Fig. 10 — the inductance fit is mostly sensitive to the S loop screening parameter $\beta = LI_c/\Phi_0$, independent of the thermopower amplitude. We find the best fit with $L \approx 50$pH. This is close to the lower limit of $L \approx 40$pH estimated from the shift of the magnetoresistance oscillations in the presence of the supercurrent applied from a power supply connected to S_3-S_4.[2] There was no hysteresis in either magnetoresistance or thermopower oscillations versus applied magnetic flux. For L=50pH and I_c=6μA the screening parameter $\beta = 0.15$. According to theory,[24] one sees hysteresis when $\beta > 1/\pi$, so the above estimation of L is consistent with the absence of hysteresis.

In Fig. 7, we plot the measured thermovoltage oscillations at three different temperatures, along with similar normalized theory curves as in Fig. 6

[2]Note that this only gives a lower limit, as only part of the supercurrent between S_3 and S_4 enters the superconducting loop.
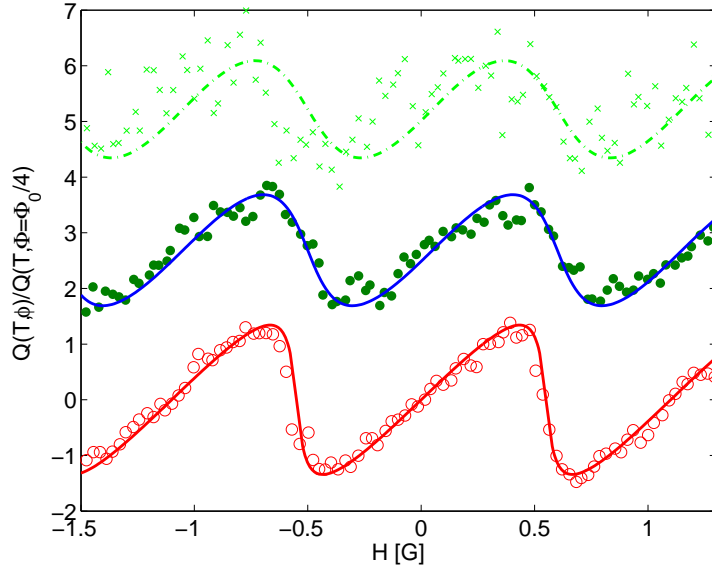
Fig. 7. (Color online): Measured thermovoltage oscillations at three different temperatures, from bottom to top: $T = 0.28$ K, $T = 0.5$ K and $T = 0.7$ K. The curves have been offset for clarity and normalized to the values at $\Phi = \Phi_0/4$. The solid lines on top of the data are the corresponding theory curves calculating with the inductance $L = 50$ pH. One should pay attention only to the shape of the curves. The temperature dependence of the measured thermopower amplitude is separately compared to the theory in Fig. 10.

with $L = 50$pH. The temperature dependence of the oscillation amplitude is compared to the theory separately, see below.

Figure 8 shows a temperature increase of the central part of interferometer T_m as a function of dc heater current at different temperatures. This was measured by comparing temperature dependence of the resistance of the N wire, measured using current contacts S_3-N_1 and potential contacts S_2-N_2, to the dependence of that on the dc heating current (see also Refs. 8,9,11). Measurements using the critical current of an SNS junction give similar dependences. The solid lines represent an approximation of low heating current part of the curve to a dependence $T_m = T_0 + aI^2$, where a is a constant, which is valid when $aI^2 \ll T_0$. The values of $2a = d^2T_m/dI^2$ are shown in Fig. 9. However, in order to calculate thermopower we need to use values of $2a^* = d^2T_h/dI^2$, where T_h is the temperature of the "hot" end of the structure, which in our case is the normal quasi-reservoir (see Fig. 1). Numerical simulation based on the actual geometry and values of resistances R_1 - R_5,
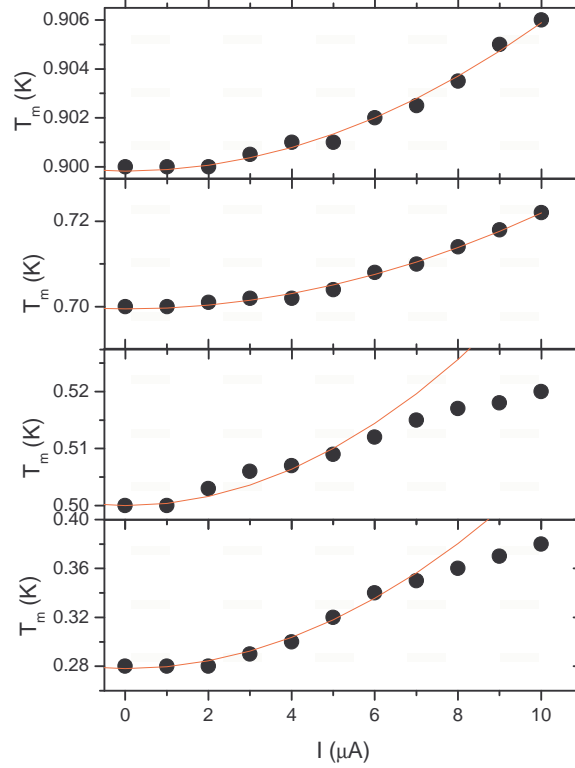
Fig. 8. (Color online): Temperature rise in the middle of the interferometer as function of heater current H_1-H_2, measured at $T = 0.28$ K, 0.5 K, 0.7 K, and 0.9 K

which also took into account the error in measuring T_m using the above method due to the difference in the interferometer resistance heated uniformly compared to that in the temperature gradient, showed that $a^* \approx 4a$, which was accurate within 10% in the whole temperature range used. Now we can convert the measured thermovoltage into thermopower. Thermovoltage measured at the frequency f of the ac modulation part of heating current is given by

$$V_f = \frac{dV}{dI}I_{ac} = Q\frac{dT_h}{dI}I_{ac} = Q2a^*I_{dc}I_{ac}, \tag{16}$$

where I_{dc} and I_{ac} are dc and ac components of the heating current, respectively. Thermovoltage measured at the frequency $2f$ in case of $I_{dc} = 0$ can be presented as (see also Ref. 8).

$$V_{2f} = \frac{1}{2}\frac{d^2V}{dI^2}\left(\frac{1}{2}I_{ac}^2\right) = \frac{1}{4}Q\frac{d^2T_h}{dI^2}I_{ac}^2 = \frac{1}{4}Q2a^*I_{ac}^2. \tag{17}$$

Note that the extra factor $1/2$ in (17) arises from the relation $I_{ac}^2 \cos^2 ft = (1/2)I_{ac}^2 + (1/2)I_{ac}^2 \cos 2ft$, so that lock-in amplifier output at $2f$ is proportional to $(1/2)I_{ac}^2$.

We have measured thermopower using both methods and found the two in a reasonable agreement. For example, for $T = 0.28$ K we found $Q_f = 1.2$ μV/K and $Q_{2f} = 0.9$ μV/K. In the range of heating currents $I_h < 10\mu A$, both V_f and V_{2f} always had symmetry of $\sin\phi$ and showed no phase-independent component observed in other experiments.

Figure 10 shows the value of thermopower as a function of bath temperature. The thermovoltage in this case was measured at $2f$ with $I_{dc} = 0$ and $I_{ac} = 6\mu A$. Magnetic field during this measurement was such that $\Phi = \Phi_0/2$. Q was then calculated using (17) and values of $2a$ found from Fig. 9 by a linear interpolation between the experimental data points.
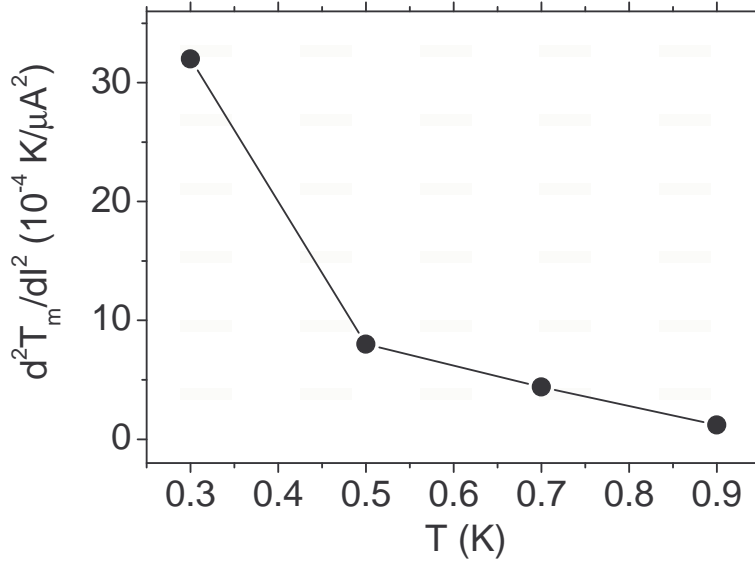

Fig. 9. Temperature dependence of the second derivative of the effective temperature rise with respect to heating current. Points are experimental data. Lines represent linear interpolation used in calculation of Q.

The temperature-dependent Q calculated from the theory is presented as lines in Fig. 10. Similar to the experimental data, the theory predicts a reentrant thermopower, with the maximum slightly above the Thouless energy. This is below the maximum point ~ 0.47 K found in the experiments. Increasing the Thouless energy in the simulations would lead to an improved fit of the peak position (see the dotted curve in Fig. 10), but then

the critical current data cannot be understood. In the presence of screening (finite L), at the lowest temperatures the phase does not reach the point where the maximum thermopower would be obtained, and thus the resulting thermopower is reduced, and the position of the maximum thermopower is slightly shifted to the right. However, to get the maximum near the experimentally observed value, a much larger value of L would be needed, and in this case the calculated $Q(T)$ is much wider than in the experiments.
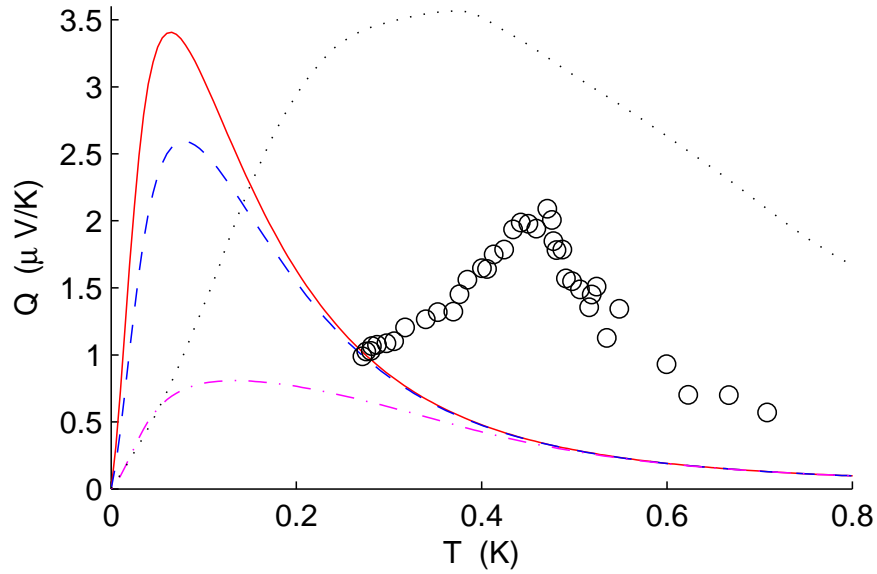

Fig. 10. (Color online): Thermopower as a function of temperature. The circles are experimental data. Lines are numerically calculated amplitudes, for $E_T/k_B = 0.05$ K and different values of the inductance: $L = 0$ (solid line), $L = 50$ pH (dashed line), and $L = 500$ pH (dash-dotted line). For comparison, similar data calculated for $E_T/k_B = 0.4$ K and $L = 0$ is plotted as a dotted line.

In the geometry of our experiment the effect of supercurrent can be measured directly. Figure 11 shows the dependence of thermovoltage on magnetic field measured at different values of dc current between contacts S_3-S_4. At small currents an extra shift in thermovoltage occurs. The precise shift depends on the ratio of the supercurrents entering the loop and flowing in the central wire. According to the simulations, the previous dominates at the temperatures where the measurements were made, and as a result the phase shift is close to $\arcsin(I_S/I_C)$.

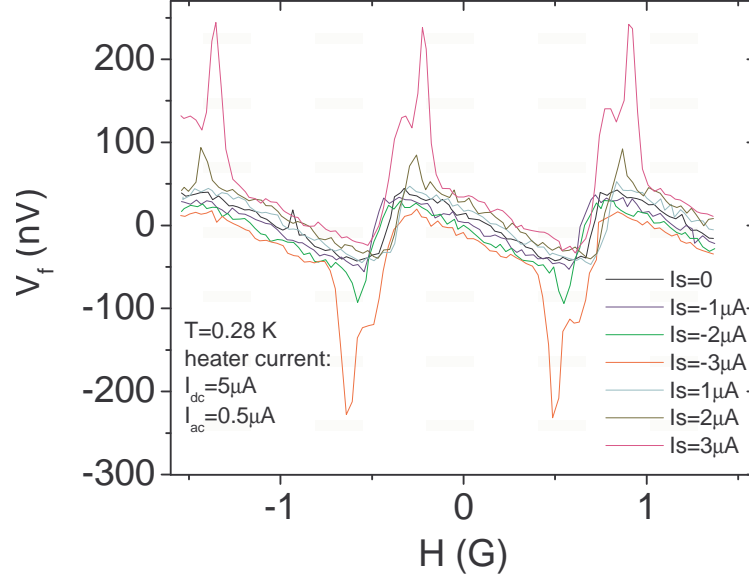Measuring V_f as a function of I_s at $H = 0$ showed linear dependence

Fig. 11. (Color online): Thermovoltage oscillations as function of magnetic field at T=0.28K at different values of dc supercurrent applied between S_3-S_4.

(see Fig. 12 and Eq. (18)). At higher values of current through S_3-S_4 the total current in the central N-wire (applied dc current plus screening current due to magnetic flux) exceeds the value of critical current of this part ($5\mu A$, see Fig. 4). In this case a dc voltage will appear between thermovoltage probes S1-N1, which is also temperature dependent. Since temperature is modulated at the frequency f, so is the above constant voltage, leading to an extra contribution to signal measured by lock-in amplifier.

Let us concentrate on the linear response to I_s. The effect of I_s can be estimated using Eq. (13). Assuming the supercurrent - phase relation in the N wire is not strongly temperature dependent, we have $I_s(T) = I_c(T)\mathrm{f}(\phi)$, where $\mathrm{f}(\phi) \approx \sin(\phi)$, Eq. (13) can be rewritten as

$$Q(I_s) = 0.58\Omega \frac{dI_s(T)}{dT} = 0.58\Omega \frac{dI_c(T)}{dT} \sin\phi = 0.58\Omega \frac{dI_c(T)}{dT} \frac{I_s}{I_c(T)}. \quad (18)$$

Substituting $dI_c/dT = 8.7 \ \mu A/K$ at $T = 0.28$ K found from Fig. 3 into (18) we get $Q = 2.5 \ \mu V/K$ for $I_s = 3 \ \mu A$. Comparing with experimental data we have $V_f(3\mu A) = 20$ nV at $I_{dc} = 5 \ \mu A$ and $I_{ac} = 0.5 \ \mu A$, which corresponds to $Q = 0.7 \ \mu V/K$. The discrepancy should be attributed to a more complicated dependence between I_s and ϕ due to the presence of the S loop.

Low-temperature thermopower in mesoscopic N/S structures
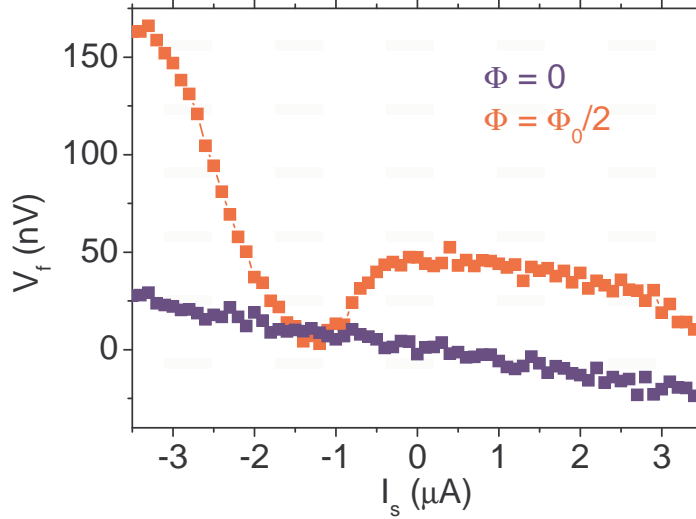

Fig. 12. (Color online): Thermovoltage as function of dc supercurrent applied between S_3-S_4 at T=0.28K. Blue: magnetic field corresponds to a zero flux through the S loop. Red: magnetic field corresponds to a half flux quantum.

5. Analysis and Discussion

We have explored the dependence of the thermopower of an Andreev interferometer on supercurrents created by magnetic field and applied directly from external power supply. The experimental thermopower was modelled theoretically using the numerical calculations with the actual geometry and fitting only the Thouless energy corresponding to the distance between the superconductors. We find that the thermovoltage oscillates as a function of the magnetic flux through the superconducting loop. The shape of these oscillations can be well described by the theory once the loop inductance is taken into account. The theory predicts correct order of magnitude for the thermopower. However, the calculated temperature dependence does not fit experimental data. The discrepancy can be attributed to the experimental error in calculating Q due to the ambiguity in determination of true temperature difference across the interferometer using only one thermometer in the middle of the structure as opposed to two separate thermometers at hot and cold ends of the interferometer. Another possible reason is a complicated geometry with its extra superconducting electrodes S_3 and S_4 in addition to the S loop, and especially the ambiguity in determining the parameters for the sample geometry.

The effect of supercurrent has been measured directly using extra super-conducting electrodes. The experimental dependence is linear in agreement with theory. The absolute value of thermopower due to this supercurrent found experimentally is smaller than that predicted by theory. This dicrepancy may at least partially be attributed to a more complicated relation between Q and I_s due to the presence of the S loop. When both externally applied supercurrent and screening current due to magnetic flux through the S loop are present, the situation becomes more complicated (see red curve in Fig. 12). In particular, when the total current approaches the critical value of the N wire, the dependence of the thermovoltage on I_s becomes strongly nonlinear. This cannot be accounted for completely by only the above mentioned extra contribution to measured signal. This case will be discussed in detail elsewhere.

When $I_h < I_c$, the quasi-reservoir is heated locally so that its distribution function is close to equilibrium. The main heat transport channel is through the N-wire into N reservoir, so that in this regime the temperature gradient is well defined. We concentrated on this regime to compare obtained results with the theoretical calculations. When $I_h > I_c$ (or when the heater electrodes made of a normal metal) heater contacts turn normal and the quasi-reservoir distribution function has a nonequilibrium form due to a long energy relaxation length in mesoscopic conductors. The measurements in this regime will be reported elsewhere.

ACKNOWLEDGMENTS

REFERENCES

1. F. Giazotto, T. T. Heikkilä, A. Luukanen, A. M. Savin, and J. P. Pekola, Rev. Mod. Phys. **78**, 217 (2006).
2. P. Virtanen and T. Heikkilä, J. Low Temp. Phys. **136**, 401 (2004).
3. N.R. Claughton and C.J. Lambert, Phys. Rev. B **53**, 6605 (1996).
4. J. Eom, C.-J. Chien, and V. Chandrasekhar, Phys. Rev. Lett. **81**, 437 (1998).
5. C.J. Lambert and R. Raimondi, J. Phys.: Condens. Matt. **10**, 901 (1998).
6. R. Seviour and A.F. Volkov, Phys. Rev. B **62**, 6116 (2000).
7. P. Virtanen and T. Heikkilä, Phys. Rev. Lett. **92**, 177004 (2004).
8. D. A. Dikin, S. Jung, and V. Chandrasekhar, Europhys. Lett. **57**, 564 (2002).

Low-temperature thermopower in mesoscopic N/S structures

9. Z. Jiang, H. Lim, V. Chandrasekhar, and J. Eom, Appl. Phys. Lett. **83**, 2190 (2003).
10. Z. Jiang and V. Chandrasekhar, Chin. J. Phys. (Taipei) **43**, 693 (2005).
11. A. Parsons, I. Sosnin, and V.T. Petrashov, Phys. Rev. B **67**, 140502 (2003).
12. A. Parsons, I. Sosnin, and V.T. Petrashov, Physica E **18**, 316 (2003).
13. V.R. Kogan, V.V. Pavlovskii, and A.F. Volkov, Europhys. Lett. **59**, 875 (2002).
14. G. Srivastava, I. Sosnin, V.T. Petrashov, Phys. Rev. B **72**, 012514 (2005).
15. Z. Jiang and V. Chandrasekhar, Phys. Rev. B **72**, 020502 (2005).
16. Z. Jiang and V. Chandrasekhar, Phys. Rev. Lett. **94**, 147002 (2005).
17. See for instance: *Proc. VIII European Symposium on Materials and Fluid Sciences in Microgravity, Brussels, Belgium* (1992), article by R.A. Wilkinson et al. and references therein.
18. C. Pittman, T. Doiron and H. Meyer, *Phys. Rev. B* **20**, 3678 (1979).
19. M. Gitterman and V.A. Steinberg, *High Temp Physics* **10**, 565 (1972) and M. Gitterman, *Rev. Mod. Phys.* **50**, 85 (1978).
20. K. D. Usadel, *Phys. Rev. Lett.* **25**, 507 (1970).
21. Y. V. Nazarov, *Superlatt. Microstruct.* **25**, 1221 (1999).
22. D.A. Dikin, S. Jung, and V. Chandrasekhar, Phys. Rev. B **65**, 012511 (2002).
23. W. Belzig, F. K. Wilhelm, C. Bruder, G. Schön, and A. D. Zaikin, *Superlatt. Microstruct.* **25**, 1251 (1999).
24. M. Tinkham, *Introduction to Superconductivity*, 2nd ed. (McGraw-Hill, New York, 1996).
25. V.T. Petrashov, R. Shaikhaidarov, and I. Sosnin, JETP Lett. **64**, 839 (1996).
26. W. Belzig, R. Shaikhaidarov, V. T. Petrashov, and Yu. V. Nazarov, Phys. Rev. B **66**, 220505(R) (2002).
27. J. E. Mooij and C. J. P. M. Harmans. *New J. Phys.* **7**, 219 (2005).